Available online at www.sciencedirect.com
ScienceDirect
Earth and Planetary Science Letters 256 (2007) 604–616
EPSL
www.elsevier.com/locate/epsl

# Nd isotopes of siliciclastic rocks from Tibet, western China: Constraints on provenance and pre-Cenozoic tectonic evolution

Kai-Jun Zhang [a,b,*], Yu-Xiu Zhang [a,c], Bing Li [a,c], Li-Feng Zhong [a,d]

[a] Guangzhou Institute of Geochemistry, Laboratory of Marginal Sea Geology, Chinese Academy of Sciences, Wushan, Guangzhou 510640, China
[b] Department of Earth Sciences, Nanjing University, Nanjing 210093, China
[c] Graduate School, Chinese Academy of Sciences, Beijing 100008, China
[d] College of Earth Sciences and Land Resources, Chang'an University, Xi'an 710054, China

Received 7 September 2006; received in revised form 5 February 2007; accepted 6 February 2007
Available online 11 February 2007
Editor: R.D. van der Hilst

**Abstract**

Nd isotope data from pre-Cenozoic siliciclastic rocks from Tibet are used to determine variations of source regions with time and hence tectonic history. On average, the $T_{DM}$ and $T_{CHUR}$ ages of the Tibetan samples are up to 1.83±0.36 Ga and 1.25±0.45 Ga, respectively, indicating that Tibet is underlain by Lower Proterozoic basement and has close affinity with the Himalayas. An Nd isotope crisis occurred at the Early Permian, with older samples defining a trend of slight decrease in $\varepsilon_{Nd}$ values with time while the Lower Permian rocks sharply increasing ~6.5 $\varepsilon_{Nd}$ units. This is related to the coeval widespread basaltic magmatism in Tibet, which could be responsible for Tibet rifting away from northern Gondwanaland. The central Qiangtang meta-sedimentary samples have distinct Nd isotope characteristics ($\varepsilon_{Nd}(0)$ −19.87±1.51; $T_{DM}$ 2.07±0.13 Ga; $T_{CHUR}$ 1.78±0.21 Ga) from the Songpan–Ganzi samples ($\varepsilon_{Nd}(0)$ −12.77±2.87; $T_{DM}$ 1.49±0.18 Ga; $T_{CHUR}$ 1.08±0.23 Ga), suggestive that these two groups were derived from different sources and that the former were not the equivalents of the latter that was underthrust from the Jinsa suture and may represent subducted continental crust. The Mid-Jurassic flysch rocks in northern Lhasa have typical upper crust Nd isotopic signatures and could have formed under a passive margin environment. Their Bangong counterparts, averagely 6.35 units higher in $\varepsilon_{Nd}$ values, unveil derivations from a likely magmatic arc along the northern Bangong margin. Basaltic pebble with low Nd content and $\varepsilon_{Nd}$ value from the Berriasian–Valanginian rocks in central Tibet, along with the samples with generally high $\varepsilon_{Nd}$ values, shows that the Bangong ophiolites could have been a main source of sediments during the earliest Cretaceous time. A significant transition of sediment sources occurred at the beginning of the Hauterivian Stage (~120 Ma). Sedimentary basaltic tuff ($\varepsilon_{Nd}(t)$2.27) in the Hauterivian–Lower Cenomanian samples in central Tibet, and common Nd signatures for input of mantle-like materials in these rocks, indicate that mantle-derived magmatic rocks could have constituted a significant source. The huge Hauterivian–Lower Cenomanian sediments in central Tibet are thus inferred to have been accumulated under a (back-arc) rifting setting.


*Keywords:* Sm–Nd isotopes; provenance; tectonics; Tibet; sediments

## 1. Introduction

The Tibetan plateau represents a major part of the Tethyan orogenic collage [1–4]. Many key aspects

* Corresponding author. Guangzhou Institute of Geochemistry, Laboratory of Marginal Sea Geology, Chinese Academy of Sciences, Wushan, Guangzhou 510640, China. Tel.: +86 20 85290232; fax: +86 20 85290130.
*E-mail address:* kaijun@gig.ac.cn (K.-J. Zhang).

0012-821X/$ - see front matter © 2007 Elsevier B.V. All rights reserved.
doi:10.1016/j.epsl.2007.02.014

about the pre-Cenozoic tectonism of Tibet still remain open to intense debate. Among them include, for example, the nature and origin of the central Qiangtang metamorphic belt (e.g. [4–8]), the structure and evolution of the Bangong–Nujiang suture (e.g. [9–13]), and role of the Late Mesozoic Lhasa–Qiangtang collision in the growth of the plateau (e.g. [4,14–16]), etc. This has impeded our understanding of the evolution of the Tethys.

In recent years, Nd isotopic systematics has been proven to be a powerful tool for investigating the sources and the tectonic significance of sedimentary rocks (see reviews [17–19]). These rocks may provide information on the provenance and, hence, crustal growth as well as orogenesis (e.g. [19,20]). In this study Nd isotopic data from pre-Cenozoic siliciclastic sediments from critical horizons from various tectonic entities in Tibet, western China have been analyzed, in an attempt to determine variations of source regions with time and hence tectonic history.

## 2. Geologic setting

From north to south, Tibet is comprised of the Songpan–Ganzi flysch complex, Qiangtang, and Lhasa terranes, which are separated by the east-striking Jinsa and Bangong–Nujiang suture zones, respectively (Fig. 1) [1–4,11–13]. The paleo-Tethys represented by the present Jinsa suture opened possibly in Early Carboniferous time [21] and closed by latest Triassic time [2,3]. On its north, the Songpan–Ganzi complex is a thick pile of deformed Ladinian through Norian (~230–203 Ma) turbidites [22].

The >500-km-long central Qiangtang metamorphic belt is a prominent feature in northern Tibet (Fig. 1). It has been proposed to represent an ultrahigh-pressure eclogite-bearing continental collision belt between the eastern and western Qiangtang blocks (Fig. 1) [8], or alternatively to contain a large metamorphic core complexes northerly underthrust from the Jinsa suture [4–6]. The eastern Qiangtang block is dominantly covered by Upper Triassic–Upper Jurassic marine intercalated siliciclastic rocks and limestones, with Carboniferous–Permian shelf strata cropped out in its easternmost margin [12,23,24]. In contrast, western Qiangtang is occupied by Carboniferous–Permian shelf strata, with Jurassic marine rocks exposed in its northern and southern limbs [12,23–25]. Therefore, structurally, Qiangtang can be regarded as a large-scale anticlinorium [4], with the central segment occupied by an anticline composed of pre-Jurassic strata and the northern and southern limbs by synclines largely made up of Jurassic sedimentary rocks. Abundant late Paleozoic tillites and glaciomarine faunas have been documented in these Carboniferous–Permian strata in the Qiangtang terrane (e.g. [13,25–27] and references therein).

The mid-Tethys branch between the Lhasa and Qiangtang terranes was open by about Permian [1,3] or

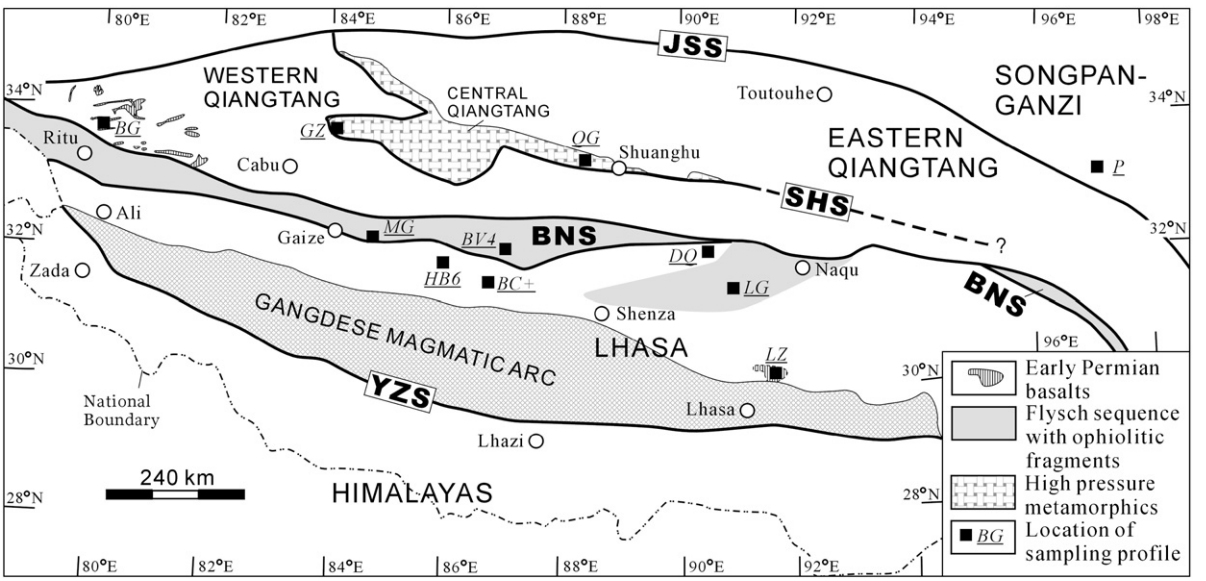


Fig. 1. Sketch tectonic map of Tibet, western China, after [12] and our own observations. Also shown are the sampling locations. Note that only shown are the Early Permian basalts that are located near the sampling profiles (BG and LZ). Sutures: BNS—Bangong–Nujiang suture; JSS—Jinsa suture; SHS—Shuanghu suture; YZS—Yarlung–Zangpo suture.

Early Jurassic time [26] and closed along the Bangong–Nujiang suture during Late Jurassic time [3,9]. This suture zone is filled by the Jurassic flysch sequence and sporadic ophiolitic fragments (Figs. 1 and 2) [12]. The Lhasa terrane can be divided into a continental Lhasa block in the north and a magmatic arc (Gangdese arc) in the south (Fig. 1) [12]. The northern Lhasa block is discriminated from its southern counterpart by extensive, late Mesozoic (mainly Cretaceous), back-arc basin sequences [12,15,16,23,24,28], and contains scattered outcrops of Paleozoic shelf sediments with the Middle Ordovician as known oldest sedimentary unit (Fig. 2) [12]. Also exposed over Jurassic flysch series are numerous ophiolitic fragments, which have been interpreted as relict of overthrust sheets, transported from the Bangong–Nujiang suture [2,9,10], or as markers of an intra-Lhasa suture [11,13,29]. In particular, the ophiolitic fragments are widespread in the area between the Naqu–Shenza to the Bangong–Nujiang suture zone (Fig. 1) [9,10].

It is generally inferred that the Lhasa block was separated from the Gondwanan supercontinent around Triassic/Jurassic boundary times (e.g. [1,3]). During Jurassic and Cretaceous time, a relatively wide passive continental margin existed along the northern rim of the Indian plate (e.g. [12,26]). During latest Cretaceous and earliest Tertiary time, the Indian subcontinent collided with the amalgamated Eurasian continent. Since about 50 Ma [1–3] or even 70 Ma [4], northward indentation of India has led to approximately 2000 km of crustal shortening, giving rise to the Tibetan plateau.

## 3. Samples and methods

A sketch of pre-Cenozoic stratigraphic data in Tibet and sampling horizons in this study is shown in Fig. 2. All eleven sampling profiles covered critical pre-Cenozoic horizons across main tectonic entities of Tibet. Except for profiles QG and GZ in central Qiangtang and profile P in Songpan–Ganzi, the other eight sampling profiles are with fine biostratigraphic control. For profiles BC+, BV4, and HB6 in central Tibet, a detailed description of petrography, stratigraphy and lithofacies has been given by [15,16]. The samples from profiles GZ, LG, MG, P, and QG are lithologically homogeneous slate or schists. Most samples from other profiles represent fresh, unmetamorphosed exposures.

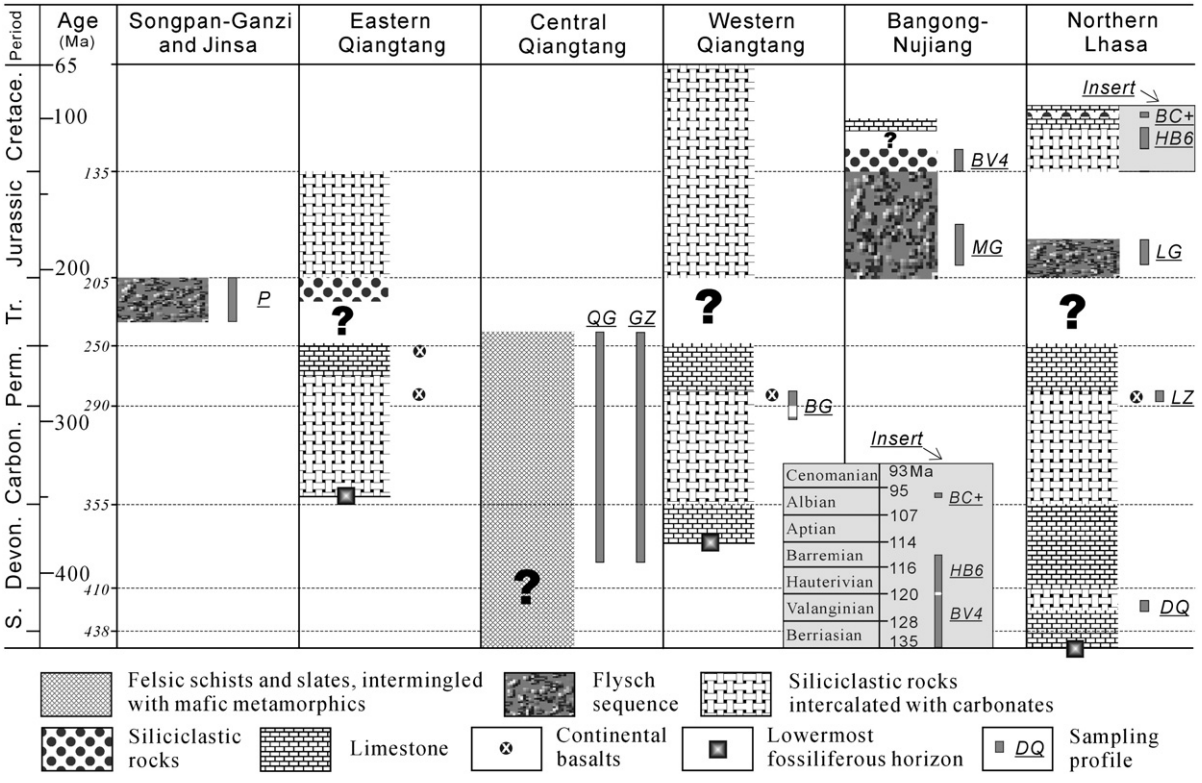


Fig. 2. A sketch of pre-Cenozoic stratigraphic data in Tibet and sampling horizons in this study. Not drawn to scale. The time intervals are after Cowie and Bassett [30]. The age of the meta-sedimentary rocks in the central Qiangtang metamorphic belt is unknown, but should be older than 240 Ma, for the ultrahigh-pressure metamorphism that occurred at about 240 Ma [8].

Table 1
Nd isotope data of pre-Cenozoic siliciclastic rocks from Tibet

| Sample | Rock type | Period | Age (Ma) | Sm (ppm) | Nd (ppm) | $^{147}Sm/^{144}Nd$ | $^{143}Nd/^{144}Nd$ | $\pm 2\sigma$ | $T_{DM}$ [a] (Ga) | $T_{chur}$ (Ga) | $\varepsilon_{Nd}(t)$ | $\varepsilon_{Nd}(0)$ |
|---|---|---|---|---|---|---|---|---|---|---|---|---|
| *Songpan–Ganzi, profile P* | | | | | | | | | | | | |
| P0 | Slate | Late Triassic | 210 | 4.72 | 26.22 | 0.1089 | 0.512078 | 10 | 1.40 | 0.97 | −8.57 | −10.92 |
| P2 | Slate | Late Triassic | 210 | 4.28 | 23.65 | 0.1094 | 0.512082 | 8 | 1.40 | 0.97 | −8.50 | −10.84 |
| P9 | Slate | Late Triassic | 210 | 4.76 | 26.09 | 0.1102 | 0.511932 | 8 | 1.63 | 1.24 | −11.47 | −13.78 |
| P12 [b] | Slate | Late Triassic | 210 | 4.10 | 22.53 | 0.1101 | 0.512134 | 9 | 1.34 | 0.89 | −7.51 | −9.83 |
| P13 | Slate | Late Triassic | 210 | 4.52 | 25.62 | 0.1066 | 0.512187 | 9 | 1.22 | 0.76 | −6.39 | −8.80 |
| P2-8 | Slate | Late Triassic | 210 | 6.75 | 39.66 | 0.1029 | 0.511792 | 9 | 1.72 | 1.37 | −13.99 | −16.49 |
| P2-11 | Slate | Late Triassic | 210 | 4.97 | 28.07 | 0.1070 | 0.511872 | 9 | 1.67 | 1.30 | −12.55 | −14.95 |
| P4-2 | Slate | Late Triassic | 210 | 3.02 | 16.06 | 0.1135 | 0.512153 | 8 | 1.35 | 0.89 | −7.23 | −9.46 |
| P4-11 | Slate | Late Triassic | 210 | 5.67 | 32.57 | 0.1053 | 0.511858 | 9 | 1.66 | 1.30 | −12.77 | −15.21 |
| Average [c] | | | | | | | | | 1.49 | 1.08 | −10.38 | −12.77 |
| *Central Qiangtang, profile GZ* [d] | | | | | | | | | | | | |
| GZ-18 | Schist | Unknown | | 5.12 | 29.98 | 0.1031 | 0.511555 | 10 | 2.05 | 1.76 | | −21.13 |
| GZ-19 | Schist | Unknown | | 5.75 | 30.98 | 0.1121 | 0.511643 | 11 | 2.10 | 1.79 | | −19.41 |
| GZ-20 | Schist | Unknown | | 4.65 | 23.49 | 0.1198 | 0.511675 | 10 | 2.23 | 1.90 | | −18.79 |
| GZ-21 | Schist | Unknown | | 3.94 | 23.09 | 0.1031 | 0.511648 | 11 | 1.92 | 1.61 | | −19.30 |
| GZ-22 | Schist | Unknown | | 4.35 | 26.77 | 0.0982 | 0.511634 | 10 | 1.86 | 1.55 | | −19.58 |
| GZ-24 | Schist | Unknown | | 5.45 | 32.04 | 0.1028 | 0.511548 | 10 | 2.06 | 1.76 | | −21.25 |
| GZ-25 | Schist | Unknown | | 3.78 | 22.47 | 0.1015 | 0.511606 | 10 | 1.95 | 1.65 | | −20.14 |
| GZ-26 [b] | Schist | Unknown | | 6.75 | 37.65 | 0.1084 | 0.511626 | 14 | 2.05 | 1.74 | | −19.74 |
| GZ-27 | Schist | Unknown | | 14.65 | 67.55 | 0.1311 | 0.511632 | 9 | 2.62 [b] | 2.33 | | −19.63 |
| GZ-28 | Schist | Unknown | | 6.79 | 36.49 | 0.1125 | 0.511605 | 8 | 2.17 | 1.86 | | −20.15 |
| GZ-29 | Schist | Unknown | | 5.33 | 29.23 | 0.1103 | 0.511588 | 10 | 2.15 | 1.85 | | −20.49 |
| Average [c] | | | | | | | | | 2.11 | 1.80 | | −19.94 |
| *Central Qiangtang, profile QG* [d] | | | | | | | | | | | | |
| QG-1 | Schist | Unknown | | 4.85 | 26.69 | 0.1099 | 0.511587 | 9 | 2.14 | 1.84 | | −20.49 |
| QG-4 | Schist | Unknown | | 8.66 | 45.67 | 0.1146 | 0.511643 | 7 | 2.16 | 1.84 | | −19.41 |
| QG-9 | Schist | Unknown | | 2.04 | 11.01 | 0.1119 | 0.511890 | 11 | 1.73 | 1.34 | | −14.60 |
| QG-10 [b] | Schist | Unknown | | 5.95 | 32.90 | 0.1093 | 0.511621 | 10 | 2.08 | 1.77 | | −19.83 |
| QG-11 | Schist | Unknown | | 6.61 | 36.27 | 0.1102 | 0.511576 | 9 | 2.17 | 1.87 | | −20.72 |
| Average [c] | | | | | | | | | 2.05 | 1.73 | | −19.00 |
| *Western Qiangtang, profile BG* | | | | | | | | | | | | |
| BG-11 | Mudstone | Early Permian | 280 | 4.86 | 29.18 | 0.1006 | 0.512073 | 7 | 1.31 | 0.90 | −7.58 | −11.01 |
| BG-12 | Sandstone | Early Permian | 280 | 5.14 | 27.17 | 0.1144 | 0.512119 | 8 | 1.42 | 0.96 | −7.19 | −10.13 |
| BG-13 | Mudstone | Early Permian | 280 | 6.21 | 31.81 | 0.1180 | 0.512044 | 9 | 1.59 | 1.15 | −8.78 | −11.59 |
| BG-15 | Sandstone | Early Permian | 280 | 6.70 | 35.82 | 0.1130 | 0.512113 | 9 | 1.41 | 0.95 | −7.24 | −10.23 |
| BG-18 | Siltstone | Early Permian | 280 | 5.63 | 30.00 | 0.1135 | 0.512129 | 9 | 1.39 | 0.93 | −6.95 | −9.92 |
| BG-20 | Mudstone | Early Permian | 280 | 6.31 | 35.55 | 0.1073 | 0.512064 | 8 | 1.40 | 0.98 | −8.01 | −11.20 |
| BG-22 | Mudstone | Early Permian | 280 | 5.81 | 29.00 | 0.1212 | 0.512055 | 10 | 1.62 | 1.18 | −8.67 | −11.36 |
| BG-24 [b] | Mudstone | Early Permian | 280 | 5.90 | 30.10 | 0.1185 | 0.512069 | 9 | 1.56 | 1.11 | −8.31 | −11.10 |
| BG-25 | Mudstone | Early Permian | 280 | 5.20 | 29.80 | 0.1054 | 0.511990 | 8 | 1.48 | 1.08 | −9.38 | −12.64 |
| Average [c] | | | | | | | | | 1.46 | 1.03 | −8.01 | −11.02 |
| BG-C | Shale | Late Carbon. | 300 | 4.29 | 23.32 | 0.1113 | 0.511669 | 9 | 2.05 | 1.72 | −15.64 | −18.90 |

*(continued on next page)*

Table 1 (*continued*)

| Sample | Rock type | Period | Age (Ma) | Sm (ppm) | Nd (ppm) | $^{147}Sm/^{144}Nd$ | $^{143}Nd/^{144}Nd$ | $\pm 2\sigma$ | $T_{DM}$ [a] (Ga) | $T_{chur}$ (Ga) | $\varepsilon_{Nd}(t)$ | $\varepsilon_{Nd}(0)$ |
|---|---|---|---|---|---|---|---|---|---|---|---|---|
| *Bangong–Nujiang, profile MG* | | | | | | | | | | | | |
| MG1 | Slate | Middle Jurassic | 180 | 4.40 | 19.31 | 0.1378 | 0.512219 | 11 | 1.65 [e] | 1.08 | −6.82 | −8.17 |
| MG2 [b] | Slate | Middle Jurassic | 180 | 3.27 | 12.67 | 0.1561 | 0.512126 | 11 | 2.44 [e] | 1.91 | −9.06 | −9.99 |
| MG3 | Slate | Middle Jurassic | 180 | 4.89 | 18.70 | 0.1581 | 0.512217 | 12 | 2.27 [e] | 1.66 | −7.33 | −8.22 |
| MG4 [b] | Slate | Middle Jurassic | 180 | 4.81 | 21.52 | 0.1352 | 0.512194 | 11 | 1.64 [e] | 1.10 | −7.25 | −8.66 |
| MG5 | Slate | Middle Jurassic | 180 | 3.88 | 15.76 | 0.1490 | 0.512157 | 12 | 2.09 [e] | 1.53 | −8.29 | −9.38 |
| Average [c] | | | | | | | | | | 1.55 | −7.62 | −8.78 |
| *Bangong–Nujiang, profile BV4* | | | | | | | | | | | | |
| BV4p [b] | Basalt pebble | Berriasian–Valanginian | 130 | 2.68 | 11.17 | 0.1451 | 0.512603 | 11 | 0.98 [e] | 0.10 | 0.18 | −0.67 |
| BV4-1 | Mudstone | Berriasian–Valanginian | 130 | 6.30 | 34.90 | 0.1093 | 0.512119 | 10 | 1.35 | 0.90 | −8.67 | −10.12 |
| BV4-2 | Siltstone | Berriasian–Valanginian | 130 | 3.72 | 19.05 | 0.1179 | 0.512253 | 11 | 1.26 | 0.75 | −6.21 | −7.52 |
| BV4-4 | Sandstone | Berriasian–Valanginian | 130 | 4.44 | 19.99 | 0.1345 | 0.512181 | 12 | 1.65 [e] | 1.12 | −7.88 | −8.91 |
| BV4-5 | Sandstone | Berriasian–Valanginian | 130 | 3.64 | 18.16 | 0.1213 | 0.512417 | 13 | 1.04 | 0.45 | −3.07 | −4.32 |
| Average [c] | | | | | | | | | 1.21 | 0.80 | −6.88 | −8.17 |
| *Lhasa, profile DQ* | | | | | | | | | | | | |
| DQ-S1 | Shale | Middle Silurian | 420 | 4.41 | 24.64 | 0.1082 | 0.511740 | 12 | 1.88 | 1.54 | −12.78 | −17.52 |
| DQ-S2 | Shale | Middle Silurian | 420 | 4.52 | 25.63 | 0.1067 | 0.511731 | 12 | 1.87 | 1.53 | −12.88 | −17.69 |
| Average [c] | | | | | | | | | 1.88 | 1.54 | −12.83 | −17.60 |
| *Lhasa, profile LZ* | | | | | | | | | | | | |
| LZ-1 | Shale | Early Permian | 280 | 3.52 | 18.52 | 0.1150 | 0.512102 | 4 | 1.45 | 1.00 | −7.54 | −10.46 |
| LZ-2 | Shale | Early Permian | 280 | 4.46 | 21.19 | 0.1273 | 0.512083 | 7 | 1.69 | 1.22 | −8.35 | −10.83 |
| Average [c] | | | | | | | | | 1.57 | 1.11 | −7.97 | −10.65 |
| *Lhasa, profile LG* | | | | | | | | | | | | |
| LG1 | Slate | Middle Jurassic | 180 | 3.64 | 18.12 | 0.1213 | 0.511911 | 15 | 1.87 | 1.47 | −12.45 | −14.18 |
| LG2 | Slate | Middle Jurassic | 180 | 5.49 | 29.86 | 0.1110 | 0.511791 | 13 | 1.86 | 1.51 | −14.57 | −16.53 |
| LG3 | Slate | Middle Jurassic | 180 | 3.53 | 18.35 | 0.1164 | 0.511822 | 13 | 1.91 | 1.55 | −14.07 | −15.91 |
| LG4 | Slate | Middle Jurassic | 180 | 3.43 | 17.27 | 0.1200 | 0.512037 | 12 | 1.63 | 1.19 | −9.98 | −11.73 |
| LG5 | Slate | Middle Jurassic | 180 | 2.16 | 11.38 | 0.1147 | 0.511761 | 15 | 1.97 | 1.63 | −15.23 | −17.11 |
| Average [c] | | | | | | | | | 1.85 | 1.46 | −13.31 | −15.16 |
| *Lhasa, profile HB6* | | | | | | | | | | | | |
| HB6-1 | Sandstone | Hauterivian–E. Barrem. | 120 | 4.87 | 23.57 | 0.1249 | 0.512754 | 10 | 0.52 | −0.25 | 3.37 | 2.27 |

Table 1 (*continued*)

| Sample | Rock type | Period | Age (Ma) | Sm (ppm) | Nd (ppm) | $^{147}Sm/^{144}Nd$ | $^{143}Nd/^{144}Nd$ | $\pm 2\sigma$ | $T_{DM}$ [a] (Ga) | $T_{chur}$ (Ga) | $\varepsilon_{Nd}(t)$ | $\varepsilon_{Nd}(0)$ |
|---|---|---|---|---|---|---|---|---|---|---|---|---|
| *Lhasa, profile HB6* | | | | | | | | | | | | |
| HB6-2 | Mudstone | Hauterivian–E. Barrem. | 120 | 3.77 | 17.20 | 0.1325 | 0.512078 | 10 | 1.81 [e] | 1.33 | −9.94 | −10.92 |
| HB6-3 | Sandstone | Hauterivian–E. Barrem. | 120 | 4.70 | 23.94 | 0.1188 | 0.512146 | 12 | 1.44 | 0.96 | −8.40 | −9.59 |
| HB6-4 [b] | Mudstone | Hauterivian–E. Barrem. | 120 | 4.02 | 20.75 | 0.1171 | 0.512216 | 11 | 1.30 | 0.81 | −7.02 | −8.23 |
| HB6-5 | Sandstone | Hauterivian–E. Barrem. | 120 | 2.39 | 11.98 | 0.1207 | 0.512307 | 12 | 1.21 | 0.67 | −5.30 | −6.47 |
| HB6-6 | Mudstone | Hauterivian–E. Barrem. | 120 | 4.19 | 20.48 | 0.1237 | 0.512269 | 10 | 1.31 | 0.77 | −6.08 | −7.20 |
| HB6-7 | Sandstone | Hauterivian–E. Barrem. | 120 | 3.48 | 17.38 | 0.1209 | 0.512152 | 11 | 1.46 | 0.98 | −8.31 | −9.47 |
| HB6-8 | Siltstone | Hauterivian–E. Barrem. | 120 | 2.58 | 11.64 | 0.1342 | 0.512124 | 10 | 1.76 [e] | 1.25 | −9.06 | −10.02 |
| HB6-9 | Siltstone | Hauterivian–E. Barrem. | 120 | 2.68 | 11.74 | 0.1382 | 0.512306 | 12 | 1.48 [e] | 0.87 | −5.58 | −6.48 |
| HB6-10 | Sandstone | Hauterivian–E. Barrem. | 120 | 3.15 | 15.32 | 0.1242 | 0.512179 | 8 | 1.47 | 0.96 | −7.84 | −8.94 |
| Average [c] | | | | | | | | | 1.24 | 0.83 | −6.10 | −7.52 |
| *Lhasa, profile BC+* | | | | | | | | | | | | |
| BC+1 | Siltstone | Albian | 100 | 4.41 | 22.76 | 0.1171 | 0.512103 | 11 | 1.48 | 1.03 | −9.43 | −10.44 |
| BC+2 | Siltstone | Albian | 100 | 4.51 | 19.33 | 0.1410 | 0.512312 | 11 | 1.53 [e] | 0.89 | −5.66 | −6.37 |
| BC+3 [b] | Siltstone | Albian | 100 | 13.41 | 67.53 | 0.1201 | 0.512184 | 10 | 1.40 | 0.90 | −7.89 | −8.86 |
| Average [c] | | | | | | | | | 1.44 | 0.94 | −7.81 | −8.75 |

[a] The model ages $T_{DM}$ were calculated following the model of DePaolo [32].

[b] Duplicate analysis.

[c] The $T_{DM}$ value labeled unrealistic model age was not included in the calculation of the average $T_{DM}$ value; weighted average $\varepsilon_{Nd}$ of $i$ samples was calculated:

$\varepsilon_{Nd} = \Sigma(\varepsilon_{Nd} \cdot [Nd]_i)/\Sigma[Nd]_i)$, where [Nd] is the Nd concentration.

[d] The age of the meta-sedimentary rocks in the central Qiangtang metamorphic belt is unknown, but should be older than 240 Ma, for the ultrahigh-pressure metamorphism that occurred at about 240 Ma [8].

[e] Unrealistic model age probably due to elevated Sm/Nd ratio.

Care was taken in sampling in all the profiles in order to avoid hydrothermal alteration and mineralization.

Fresh rock samples were powdered to 200 mesh in an agate mill to avoid contamination. The Nd isotopic ratios were measured with a Micromass IsoProbe™ multiple-collectors inductively coupled plasma-mass spectrometer (MC-ICPMS) at the Isotopic Laboratory of Guangzhou Institute of Geochemistry, Chinese Academy of Sciences. The analytical technique followed Liang et al. [31]. The analytical errors were less than 0.002% for $^{143}Nd/^{144}Nd$. Total procedural Nd blanks were less than 70 pg during the period of sample analysis. The accuracy of the concentrations and the Sm/Nd ratios was better than 2% and the reproducibility of $^{143}Nd/^{144}Nd$ ratios was less than $2.5 \times 10^{-6}$ (2ó). These values were determined both by 20 measurements of Shin-Etsu JNDi-1 standards with $^{143}Nd/^{144}Nd$ ratios of 0.512120 (12), and by some duplicates that were melted before dissolution, which confirmed the complete dissolution of the samples in the Teflon vessels.

The Nd isotopic data determined in this study are listed in Table 1, and are graphically presented in Figs. 3 and 4. Depleted mantle model ages were calculated following the model of DePaolo [32]. The sediments analyzed are essentially fine-grained (siltstones, slates, mudstones) and some sandstones, and the differences observed for depleted mantle model ages could be an artifact of differences in mixing proportions (e.g., [33]). Therefore, we mainly employed the $\varepsilon_{Nd}$ values to determine provenance sources and tectonic setting of the sedimentary rocks in this study, with a cautious incorporation of the depleted mantle model ages. In particular, we did not

use those depleted mantle model ages for the samples with elevated $^{147}Sm/^{144}Nd$ ratios (>0.130), which may be a product of modification by secondary processes, especially diagenetic reactions [34,35].

## 4. Nd isotope data

All the nine analyzed samples from profile P in the Songpan–Ganzi complex (Figs. 1 and 2) range in $\varepsilon_{Nd}(0)$ values from −8.8 to −16.49, and have $\varepsilon_{Nd}(0)$ values of −12.77±2.87, $T_{DM}$ ages of 1.49±0.18 Ga, $T_{CHUR}$ ages of 1.08±0.23 Ga, and $^{147}Sm/^{144}Nd$ ratios of 0.108±0.003 (Table 1).

The majority of the samples from profiles GZ and QG in the central Qiangtang metamorphic belt (Figs. 1 and 2) are characterized by low $\varepsilon_{Nd}(0)$ values of −18.79 to −21.25,old $T_{DM}$ ages of >1.9 Ga and $T_{CHUR}$ ages of >1.55 Ga. One exception is sample QG-9, which yielded an $\varepsilon_{Nd}(0)$ value of −14.66, a $T_{DM}$ age of 1.73 Ga and a $T_{CHUR}$ age of 1.34 Ga. This sample also has the lowest Nd content of 11 ppm, while the Nd concentrations of other samples are generally more than 22 ppm. All these samples have an average $\varepsilon_{Nd}(0)$ value of −19.87,and average $T_{DM}$ and $T_{CHUR}$ ages of 2.07 Ga 1.78 Ga, respectively. Most of the samples have $^{147}Sm/^{144}Nd$ ratios lower than 0.115 (Table 1), which is the average value usually reported for the detrital sediments and corresponds to the average value for the upper continental crust (e.g., [36–39]).

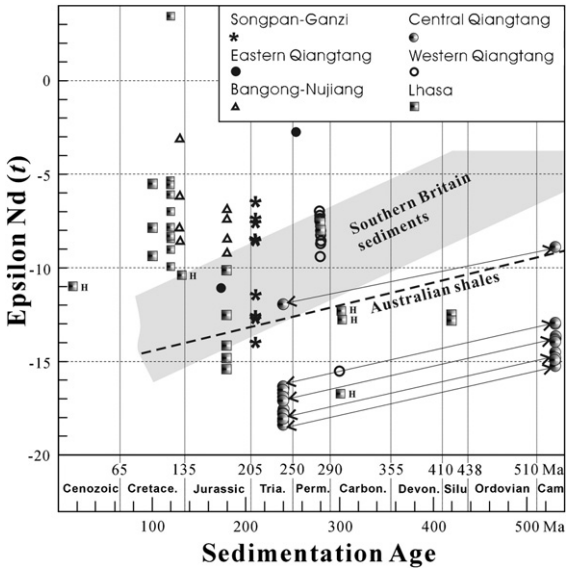


Fig. 3. Variation of $\varepsilon_{Nd}(t)$ with sedimentation ages for the pre-Cenozoic siliciclastic rocks from Tibet. The age of the meta-sedimentary rocks in the central Qiangtang metamorphic belt is unknown, but should be older than 240 Ma, for the ultrahigh-pressure metamorphism that occurred at about 240 Ma [8], and the double arrows represent the possible range of $\varepsilon_{Nd}(t)$ values of these central Qiangtang meta-sedimentary rocks. Data are from Table 1 and the time intervals after Cowie and Bassett [30]. Five Lhasa samples labeled H and two eastern Qiangtang samples are after Harris et al. [40]. The fields for the southern Britain sediments and Australian shales are after [57,58], respectively.

In the western Qiangtang block, the Lower Permian samples from profile BG (Figs. 1 and 2) produced apparently higher $\varepsilon_{Nd}(0)$ values that range from −9.92 to −12.64, with an average $\varepsilon_{Nd}(0)$ value of −11.02. These samples also have young $T_{DM}$ (1.31 to 1.62 Ga, average 1.46 Ga) and $T_{CHUR}$ (0.90 to 1.18 Ga, average 1.03 Ga) ages. Most of the samples have $^{147}Sm/^{144}Nd$ ratios lower than 0.115. In contrast, however, one Upper Carboniferous shale from the same profile (Figs. 1 and 2) exhibits much lower $\varepsilon_{Nd}(0)$ value (−18.90) and apparently older $T_{DM}$ (2.05 Ga) and $T_{CHUR}$ (1.72 Ga) ages (Table 1).

In the Bangong–Nujiang suture zone, a characteristic feature of the Mid-Jurassic flysch shale samples from profile MG (Figs. 1 and 2) is their remarkably high $^{147}Sm/^{144}Nd$ ratios that vary between 0.135 and 0.158. This suggests either that the sedimentary processes that formed these samples favor higher Sm/Nd ratios or that at least one end-member had an Sm/Nd ratio higher than the typical continental crust. These samples have $\varepsilon_{Nd}(0)$ values of −8.81±0.79 and Nd concentrations of 17.81±3.41 ppm (Table 1).

In order to determine the $\varepsilon_{Nd}$ values of the eroded rocks directly, one basaltic pebble (BV4p) extracted from pebbly sandstone in profile BV4 from the Bangong–Nujiang suture zone (Figs. 1 and 2). It yielded $\varepsilon_{Nd}(0)$ value (−0.67), high $^{147}Sm/^{144}Nd$ ratio (0.145), and very low Nd content (11.17 ppm). The other four Lower Cretaceous (Berriasian–Valanginian. Insert in Fig. 2) siliciclastic samples from this profile have changing $\varepsilon_{Nd}(0)$ values from −4.32 to −10.12 (average −8.17±2.50), $T_{DM}$ ages from 1.04 to 1.35 Ga (average 1.21±0.16 Ga), $T_{CHUR}$ ages from 0.45 to 1.12 Ga (average 0.80±0.28 Ga), and $^{147}Sm/^{144}Nd$ ratios from 0.109 to 0.134 (average 0.121±0.01). Among them, three samples have Nd contents of 18–20 ppm, and the Nd concentration of another sample is up to 34.9 ppm (Table 1).

In the Lhasa block, two Middle Silurian shales from profile DQ (Figs. 1 and 2) produced $\varepsilon_{Nd}(0)$ values of −17.52 and −17.69, $T_{DM}$ ages of 1.87 and 1.88 Ga, and $T_{CHUR}$ ages of 1.53 and 1.54 Ga, respectively. Two Lower Permian shales from profile LZ (Figs. 1 and 2) display obviously larger $\varepsilon_{Nd}(0)$ values (−10.46 and −10.83, respectively) and manifestly younger $T_{DM}$ (1.45 and 1.69 Ga, respectively) and $T_{CHUR}$ (1.00 and 1.22 Ga, respectively) ages (Table 1), and show strong similarity to

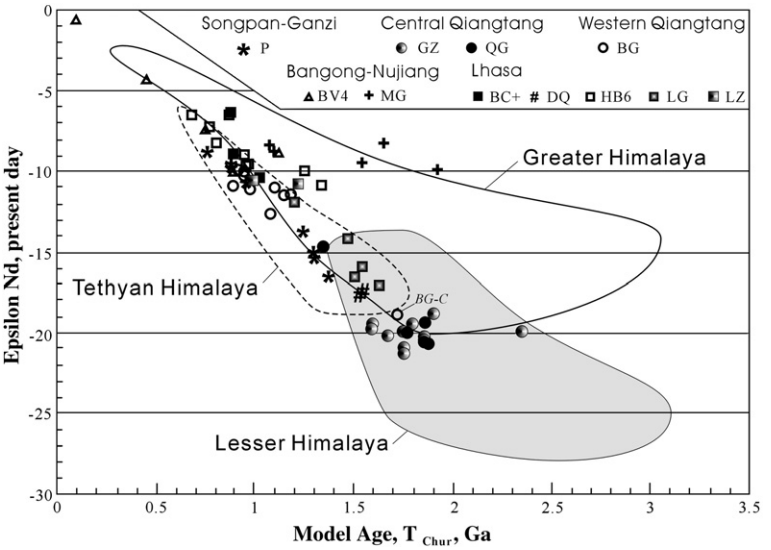


Fig. 4. $T_{CHUR}$ vs. $\varepsilon_{Nd}(0)$ diagram for the pre-Cenozoic siliciclastic rocks from Tibet. Data are from Table 1. The Himalayan fields are after [42–44] and references therein.

their equivalents in the western Qiangtang block (Fig. 3). Unlike their Bangong–Nujiang counterparts, the Middle Jurassic flysch samples from profile LG in northern Lhasa (Figs. 1 and 2) produced $^{147}Sm/^{144}Nd$ ratios of 0.117±0.004, $\varepsilon_{Nd}(0)$ values of −15.16±2.18, $T_{DM}$ ages of 1.85±0.13 Ga, and $T_{CHUR}$ ages of 1.46±0.16 Ga. Except for sample LG2 (Nd=30 ppm), other four samples exhibit Nd contents of <20 ppm. (Table 1).

Most of the samples from profile HB6 exhibit negative $\varepsilon_{Nd}(0)$ values from −6.47 to −10.92, and moderate $T_{DM}$ (from 1.26 to 1.47 Ga), and $T_{CHUR}$ (from 0.67 to 1.33 Ga) ages. One exception is sample HB6-1. It yielded a positive $\varepsilon_{Nd}(0)$ value of 2.27, a young $T_{DM}$ age of 0.68 Ga, and a negative $T_{CHUR}$ age. All the samples have $^{147}Sm/^{144}Nd$ ratios more than 0.117 (average 0.126±0.007) but Nd contents lower than 24 ppm (average 17.4±4.72 ppm). Notably, three siliciclastic samples from the rare intercalations in the Mid-Cretaceous monotonous limestones (profile BC+) show strong similarity to Nd isotope characteristics to those from profile HB6 by varying negative $\varepsilon_{Nd}(0)$ values (−8.75±2.05), young $T_{DM}$ and $T_{CHUR}$ ages (average 1.44 and 0.94 Ga, respectively), and high $^{147}Sm/^{144}Nd$ ratios (0.126±0.013).

## 5. Discussion

### 5.1. Tectonic implications of the Early Permian Nd isotope crisis

A crisis of the Nd isotopes with sedimentation ages occurred at the Early Permian (~280 Ma) (Fig. 3). Our two Mid-Silurian and one Upper Carboniferous samples, along with our meta-sedimentary rock samples from central Qiangtang and three Upper Carboniferous samples from Harris et al. [40], define a weak trend of decrease in $\varepsilon_{Nd}$ values in the younger sediments prior to the Early Permian (Fig. 3). Such a trend reveals continuous reworking of Tibetan crust prior to the Early Permian, with no introduction of younger material by either magmatic or tectonic processes. However, the Lower Permian samples from the Lhasa and Qiangtang blocks remarkably increase approximately 6.5 $\varepsilon_{Nd}$ units (Fig. 3) and therefore their $T_{DM}$ and $T_{CHUR}$ ages decrease ~0.4 Ga and ~0.5 Ga, respectively (Table 1). From then on, this increasing trend in $\varepsilon_{Nd}$ with decreasing age of sedimentation seems to be irregularly continued (Fig. 3).

This Nd isotope crisis means that there is an intense input of a juvenile mantle-derived component (e.g. [17–20]) during the deposition of the Lower Permian formations. Arc magmatism or orogenesis due to plate accretions was the dominant reason for increase of $\varepsilon_{Nd}$ values in the Songpan–Ganzi complex and the Qiangtang and Lhasa blocks in the Mesozoic [40]. However, similar tectonothermal event was lacking in these three tectonic entities at the Early Permian [12,25]. Lower Permian sandstone samples in western Qiangtang are characterized by abundant plagioclase grains (20–40 wt.%, generally Ab<50) and sporadic augite grains as well as minor basaltic lithic fragments. Because of widespread intercalations of basalt in the Lower Permian siliciclastic rocks [12,25,41], along with the above-mentioned petrographic features of the samples indicative of distinct input from these nearby basalts, we attribute the Early

Permian Nd isotope crisis to such mafic magmatism. The Early Permian basalts are widespread not only in central Qiangtang [7,8], in western Qiangtang [12,25,41], but also in Lhasa [12]. They have maximum thickness of >2000 m [41] and geochemically exhibit typical oceanic island basalt (OIB) characteristics [7,8]. We speculate that an Early Permian (~280 Ma) mantle plume upwelling event could be responsible for the Nd isotope crisis recorded in the siliciclastic rocks. This mantle plume upwelling event could have perhaps initiated not only the rifting of Tibet away from northern Gondwanaland, but also the separation of Qiangtang from Lhasa.

### 5.2. Affinity of the Tibetan basement

Tibet as the passive margin of Gondwanaland during the Paleozoic has been suggested by broad geologic studies already [2,3,12]. On average, the $T_{DM}$ age of the pre-Cenozoic siliciclastic rocks in both the Lhasa and Qiangtang blocks from this study is up to 1.65±0.36 Ga, suggestive of that Tibet is underlain by Lower Proterozoic basement. Many samples display low $\varepsilon_{Nd}(0)$ values up to −20. Moreover, the samples are overwhelmingly plotted in the field of the Tethyan, Greater, and Lesser Himalayas ([42–44] and references therein) in an $\varepsilon_{Nd}(0)$ vs. Nd model ages ($T_{CHUR}$) diagram (Fig. 4). Therefore, most likely, Tibet is underlain by Himalaya-type Early Proterozoic basement and has close affinity with the Himalayas. This is consistent with the fact that the Himalayas and the Lhasa block have similar Precambrian basement and underwent the emplacement of magmas in early Paleozoic times on the basis of U–Pb dates on zircons ([43,45,46] and references therein).

### 5.3. Origin and nature of the central Qiangtang metamorphic belt

The >500-km-long and up to 100-km-wide blueschist-bearing metamorphic belt within the Qiangtang interior, is a prominent feature in the Tibetan plateau (Fig. 1). Its origin remains open to intense debate, and has been interpreted as: (1) early Mesozoic mélange that was underthrust northerly from the Jinsa suture and then exhumed in the interior of the Qiangtang block [4–6]; (2) a Late Paleozoic rift (e.g. [47]); (3) an ultrahigh-pressure metamorphic belt produced by the Eastern and Western Qiangtang continental collision along the in situ Shuanghu suture zone [7,8]. These three main models have fundamental differences in the first-order crustal structure and accretionary history of the central Tibetan plateau [6,8,47]. The origin of the central Qiangtang metamorphic belt thus forms a key aspect for understanding the evolution of the Tethys.

A compilation of Sm–Nd data [20] shows the influence of the geodynamic locations (active or passive margins) on the isotopic compositions of the sediments. Clearly, in the present case of central Qiangtang, low and homogenous $\varepsilon_{Nd}(0)$ values (−19.87±1.51), old and uniform $T_{DM}$ (2.07±0.13 Ga) and $T_{CHUR}$ (1.78±0.21 Ga) ages, and fairly restricted $^{147}Sm/^{144}Nd$ ratios (0.110±0.008) (Table 1) indicate their cratonic/passive margin setting, old provenance, and long sedimentary recycling histories. This agrees well with the conclusions drawn from geochemical studies [7]. In contrast, the meta-sedimentary rocks from the Songpan–Ganzi Complex exhibit much higher $\varepsilon_{Nd}(0)$ values (−12.77±2.87) and younger $T_{DM}$ (1.49±0.18 Ga) and $T_{CHUR}$ (1.08±0.23 Ga) ages (Table 1). These Sm–Nd isotope data confirm earlier conclusion of old sediment sources of the Songpan–Ganzi flysch sequences based on U–Pb detrital zircon geochronology [48]. However, the distinct Sm–Nd isotope characteristics suggest that the meta-sedimentary rocks from central Qiangtang and Jinsa should have been derived from sharply various source regions and tectonic settings that have obviously different Nd isotopic characteristics [20]. The central Qiangtang metamorphic rocks should not be the equivalents of the Songpan–Ganzi flysch sequence that was northerly underthrust from the Jinsa suture during the early Mesozoic [4–6]. Because the mafic rocks intermingled with these central Qiangtang meta-sedimentary rocks have undergone (ultra) high-pressure metamorphism [8], they should represent subducted and then exhumed continental crust.

### 5.4. Structure and evolution of the Bangong–Nujiang suture zone

Intensive debates regarding the structure and evolution of the Bangong–Nujiang suture zone focus on: (1) the nature of the ophiolite massifs within the northern Lhasa blocks (Fig. 1) (overthrust sheets or in situ suture(s) (e.g. [11,13]); (2) subduction polarity of the Bangong–Nujiang Tethyan ocean (southward or northward (e.g. [21,49]); and (3) role of the Lhasa–Qiangtang collision in the growth of the Tibetan plateau (elevation by 3–4 km since 99 Ma [4,14] or negligible [15,16,24,28]).

The Nd isotopes of the Late Mesozoic siliciclastic rocks may provide useful constraints on this key issue of Tibetan tectonics. As stated above, the Mid-Jurassic flysch rocks (profile MG) in the Bangong–Nujiang suture zone possess distinct Nd isotope characteristics

from their counterparts (profile LG) in the northern Lhasa block (Fig. 3). The latter have typical upper crust $^{147}Sm/^{144}Nd$ ratios (0.117±0.004), low $\varepsilon_{Nd}(0)$ values of −15.16±2.18, and old $T_{DM}$ (1.85±0.13 Ga) and $T_{CHUR}$ (1.46±0.16 Ga) ages (Table 1), suggestive of their most likely derivations from passive margin setting. Therefore, the northern Lhasa block most likely represents a passive margin prior to the Lhasa–Qiangtang collision. The intra-Lhasa suture models for the ophiolitic slices on the northern Lhasa block is not favored here, because the Mid-Jurassic flysch sequence should have formed in an active continental margin [11] if these models were right. Compared with the latter, the former are averagely 6.35 units higher in $\varepsilon_{Nd}$ values (Table 1). This situation could have formed either by the secondary sedimentary processes [34,35] that formed the samples in the Bangong–Nujiang suture zone favoring higher Sm/Nd and/or $^{143}Nd/^{144}Nd$ ratios, or by input of at least one end-member having Sm/Nd and/or $^{143}Nd/^{144}Nd$ ratios higher than the typical continental crust [38,50]. In order to examine whether the secondary sedimentary processes have resulted in elevated $^{143}Nd/^{144}Nd$ and $^{147}Sm/^{144}Nd$ ratios of these Bangong–Nujiang samples, we analyzed the rare earth element (REE) compositions of other four samples through profile MG (Table 1 in the Appendix). These nine Bangong–Nujiang samples exhibit similar REE patterns with no Ce anomaly and no REE fractionation (Fig. 1 in the Appendix). Therefore, according to McDaniel et al. [33], it is highly impossible for the secondary sedimentary processes to have acted as a main factor for the elevation of $^{143}Nd/^{144}Nd$ and $^{147}Sm/^{144}Nd$ ratios of these Bangong–Nujiang samples. Chemical sediment and mantle-derived material are two candidates with higher Sm/Nd and/or $^{143}Nd/^{144}Nd$ ratios than the typical continental crust. However, petrographic observations did not show appreciable chemical sediments, except for $SiO_2$, in these clastic rocks. Therefore, we tend to attribute the Nd isotope characteristics of the Bangong–Nujiang samples to input of the mantle materials. A source of ophiolite for these Mid-Jurassic Bangong–Nujiang sediments deposited at ~180 Ma is absent for obduction of the ophiolite from the Bangong–Nujiang ocean occurred at ~152 Ma [51]. Therefore, it is possible that a magmatic arc along the northern margin of the Bangong–Nujiang Ocean could have provided mantle-like materials for these sediments.

The low Nd content (11 ppm) of the basaltic pebble (BV4p; Table 1) from the Berriasian–Valanginian (Lower Cretaceous) siliciclastic rocks in the Bangong–Nujiang belt, with no carbonation and silicification observed, indicates that it could not have come from the coeval arc volcanic rocks in the Lhasa block, because their Nd contents are generally more than 20 ppm (e.g. [41,52–54]). Instead, low Nd contents are a characteristic of the mafic rocks from the Bangong–Nujiang ophiolites [10,55]). Its low $\varepsilon_{Nd}(t)$ value of 0.18 (Table 1) unveils that it must have been contaminated by continental matter when it formed. Such contamination has also been identified to be widespread in the Bangong–Nujiang ophiolites [10,55]. Hence, The pebble BV4p was most likely derived from the ophiolites. The siliciclastic sample BV4-5 with high $\varepsilon_{Nd}(t)$ value of −3 (Table 1) could provide an example for mixing of the detritus from the ophiolites and the upper crustal materials, which is consistent with petrographic observations [16]. Other samples also yielded $\varepsilon_{Nd}(t)$ values higher than −8.67 (Fig. 3; Table 1). A mixing of 42–75 wt.% of mafic fragments from the Bangong–Nujiang ophiolites could well meet the Nd isotope budget of these samples, provided another end member is the average Himalayan continent crust (Sm 6.58 ppm, Nd 35.31 ppm, $\varepsilon_{Nd}$ −19; weighted average from [42–44]). Therefore, during the Berriasian–Valanginian Stages, the mafic rocks from the ophiolites in the Bangong–Nujiang suture could have been one of the main sources of siliciclastic rocks in the Bangong–Nujiang zone and the northern Lhasa block [15,16].

Because there are no basalts or other mafic rocks that were found in the neighboring areas except for the syndepositional basaltic intercalations [15,16], the positive $\varepsilon_{Nd}(0)$ value of 2.27, young $T_{DM}$ age of 0.52 Ga, and negative $T_{CHUR}$ age of sample HB6-1 from profile HB6 (Table 1) indicate it is a weakly-weathered and shortly-transported sedimentary basaltic tuff, compatible with previous conclusion based on geochemical studies [15]. Three samples from profile HB6, which contain both calcareous interstitial matrix and abundant limestone lithic fragments as observed by petrographic studies, exhibit Nd contents lower than 12 ppm but $\varepsilon_{Nd}(0)$ values from −6.47 to −10.02 (Table 1), indicating that input of limestone (Nd 5 ppm, $^{147}Sm/^{144}Nd$ 0.145, $\varepsilon_{Nd}$ −8.1; [56]), instead of addition of the mafic rocks (e.g., BV4p; low Nd content but high $\varepsilon_{Nd}$ value) from the Bangong–Nujiang ophiolites, is the reason of dilution of Nd concentrations [15]. A mixing of 13–44 wt.% of the syndepositional mafic volcanic fragments such as sample HB6-1 with the average Himalayan continent crust (10–40 wt.%) and limestone (20–70 wt.%) could well meet the Nd isotope budget of the HB6 samples. Notably, two samples from profile BC+ yielded similar Nd isotope signatures to the samples from profile HB6, including irregular variations of $\varepsilon_{Nd}$ values and $^{147}Sm/^{144}Nd$ ratios, and generally young $T_{DM}$ and $T_{CHUR}$ ages (Fig. 4; Table 1), implying that

they have similar source regions to those from profile HB6. However, sample BC+3 has strikingly high Sm and Nd concentrations (13.41 and 67.53 ppm, respectively; Table 1), very rare in the Himalayan rocks [43,44]. We interpret that this sample ($SiO_2$ 65.23 wt.%; [15]) should have received intense input from strongly fractionated rhyolitic rocks with high rare earth element (REE) contents. This is compatible with the conclusion that it represents weakly weathered sedimentary rhyolitic tuffs by previous geochemical studies [15]. Therefore, we believe that the coeval mantle-derived bimodal volcanic rocks must have played a key role in supplying the Hauterivian–Early Cenomanian clastic sediments in central Tibet. Clearly, a significant transition of sediment sources occurred at the beginning of the Hauterivian Stage (~120 Ma; [30]). This volcanism during the Hauterivian–Early Cenomanian in central Tibet was accompanied by continuous crustal subsidence that resulted in deposition of the Hauterivian–Lower Cenomanian marine sediments up to >5000 m [12,15,16]. We therefore infer that the Hauterivian–Lower Cenomanian sediments could have been accumulated under a (back-arc) rifting setting.

## 6. Conclusions

1 Sixty-seven pre-Cenozoic siliciclastic rocks from Tibet were analyzed for Nd isotopes, in an attempt to determine variations of source regions with time and hence tectonic history. On average, the $T_{DM}$ and $T_{CHUR}$ ages of the Tibetan samples are up to 1.65±0.36 Ga and 1.25±0.45 Ga, respectively. Therefore, Tibet is likely underlain by Lower Proterozoic basement and has close affinity with the Himalayas.

2 An Nd isotope crisis occurred at the Early Permian. Older samples define a weak trend of slight decrease in $\varepsilon_{Nd}$ values with time, while the Lower Permian rocks sharply increase ~6.5 $\varepsilon_{Nd}$ units. This is related to the coeval widespread basaltic magmatism in Tibet. An Early Permian mantle plume upwelling event that rifted Tibet away from northern Gondwanaland could be responsible for this basaltic magmatism.

3 The central Qiangtang meta-sedimentary samples have distinct Nd isotope characteristics ($\varepsilon_{Nd}(0)$ −19.87±1.51; $T_{DM}$ 2.07±0.13 Ga; $T_{CHUR}$ 1.78±0.21 Ga) from the Songpan–Ganzi samples ($\varepsilon_{Nd}(0)$ −12.77±2.87; $T_{DM}$ 1.49±0.18 Ga; $T_{CHUR}$ 1.08±0.23 Ga). These two groups must have been derived from different sources, and the former were not the equivalents of the latter that was underthrust from the Jinsa suture and may represent subducted continental crust.

4 The Mid-Jurassic flysch rocks in northern Lhasa have typical upper crust Nd isotopic signatures and therefore northern Lhasa could represent a passive margin setting during early Mesozoic time. Their Bangong counterparts, averagely 6.35 units higher in $\varepsilon_{Nd}$ values, unveil derivations from a likely magmatic arc along the northern Bangong margin.

5 A significant transition of sediment sources occurred at the beginning of the Hauterivian Stage (~120 Ma). During the Berriasian–Valanginian Stages, the Bangong–Nujiang ophiolites could have been a main source of sediments, as shown by ophiolite-derived basaltic pebble with low Nd content and $\varepsilon_{Nd}$ value and the samples with generally high $\varepsilon_{Nd}$ values. However, basaltic tuff in the Hauterivian–Lower Cenomanian samples, and common Nd signatures for input of mantle-like materials in these rocks, indicate that mantle-derived magmatic rocks could have constituted a significant source. Therefore, the huge Hauterivian–Lower Cenomanian sediments in central Tibet are inferred to have been accumulated under a (back-arc) rifting setting.

## Acknowledgements

This research was supported by the Natural Science Foundation of China (grant 40572137) and the Hundred Talents Project, Chinese Academy of Sciences. We are grateful to Y. Wang, Q.G. Wei, and T.P. Zhao for their assistance in fieldwork, to X.R. Liang, Y. Liu, and Y.X. Wang for their analytical support, and to U. Schärer for the constructive and thoughtful reviews, which greatly improved the paper.

## Appendix A. Supplementary data

Supplementary data associated with this article can be found, in the online version, at doi:10.1016/j.epsl.2007.02.014.

## References

[1] C.J. Allègre, et al., Structure and evolution of the Himalaya–Tibet orogenic belt, Nature 307 (1984) 17–22.
[2] C.F. Chang, et al., Preliminary conclusions of the Royal Society/Academia Sinica 1985 Geotraverse of Tibet, Nature 323 (1986) 501–507.
[3] J.F. Dewey, R.M. Shackleton, C. Chang, Y. Sun, The tectonic development of the Tibetan plateau, Philos. Trans. R. Soc. Lond., A 327 (1988) 379–413.
[4] A. Yin, T.M. Harrison, Geologic evolution of the Himalayan–Tibetan Orogen, Annu. Rev. Earth Planet. Sci. 28 (2000) 211–280.
[5] P. Kapp, A. Yin, C.E. Manning, M. Murphy, T.M. Harrison, M. Spurlin, L. Ding, X.G. Deng, C.M. Wu, Blueschist-bearing

metamorphic core complexes in the Qiangtang block reveal deep crustal structure of northern Tibet, Geology 28 (2000) 19–22.
[6] P. Kapp, A. Yin, C.E. Manning, T.M. Harrison, M.H. Taylor, Tectonic evolution of the early Mesozoic blueschist-bearing metamorphic belt, central Tibet, Tectonics 24 (2003) 1043, doi:10.1029/2002TC001383.
[7] K.J. Zhang, Y.X. Zhang, B. Li, Y.T. Zhu, R.Z. Wei, The blueschist-bearing Qiangtang metamorphic belt (northern Tibet, China) as an in situ suture zone: evidence from geochemical comparison with the Jinsa suture, Geology 34 (2006) 493–496.
[8] K.J. Zhang, J.X. Cai, Y.X. Zhang, T.P. Zhao, Eclogites from central Qiangtang, northern Tibet (China) and tectonic implications, Earth Planet, Sci. Lett. 245 (2006) 722–729.
[9] J. Girardeau, et al., Tectonic environment and geodynamic significance of the Neo-Cimmerian Dongqiao ophiolite, Bangong–Nujiang suture zone, Tibet, Nature 307 (1984) 27–31.
[10] J.A. Pearce, W.M. Deng, The ophiolites of the Tibet Geotraverses, Lhasa to Golmud (1985) and Lhasa to Kathmandu (1986), Philos. Trans. R. Soc. Lond., A 327 (1988) 218–241.
[11] K.J. Hsü, G.T. Pan, A.M.C. Sengör, Tectonic evolution of the Tibetan Plateau: a working hypothesis based on the archipelago model of orogenesis, Int. Geol. Rev. 37 (1995) 473–508.
[12] Xizang Bureau of Geology and Mineral Resources, Regional Geology of Xizang Autonomous Region, China, Geol. Publ. House, Beijing, 1993, 707 pp.
[13] P. Matte, P. Tapponnier, N. Arnaud, J. Bourjot, J.P. Avouac, P. Vidal, Q. Liu, Y. Pan, Y. Wang, Tectonics of Western Tibet, between the Tarim and the Indus, Earth Planet. Sci. Lett. 142 (1996) 311–330.
[14] M.A. Murphy, A. Yin, T.M. Harrison, S. Dürr, Z. Chen, F.J. Ryerson, W.S.F. Kidd, X. Wang, X. Zhou, Did the Indo–Asian collision alone create the Tibetan plateau? Geology 25 (1997) 719–722.
[15] K.J. Zhang, Secular geochemical variations of the Lower Cretaceous siliciclastic rocks from central Tibet (China) indicate a tectonic transition from continental collision to back-arc rifting, Earth Planet. Sci. Lett. 229 (2004) 73–89.
[16] K.J. Zhang, B.D. Xia, G.M. Wang, Y.T. Li, H.F. Ye, Early Cretaceous stratigraphy, depositional environment, sandstone provenance, and tectonic setting of central Tibet, western China, Geol. Soc. Amer. Bull. 116 (2004) 1202–1222.
[17] I.N. Clauer, S. Chaudhuri, Isotopic signatures and sedimentary records, in: N. Clauer, S. Chaudhuri (Eds.), Lecture Notes in Earth Sciences, vol. 43, 1992, 529 pp.
[18] G. Faure, Principles of Isotope Geology, 2nd ed., Wiley, New York, 1986, 589 pp.
[19] J.B. Murphy, R.D. Nance, Sm–Nd isotopic systematics as tectonic tracers: an example from West Avalonia in the Canadian Appalachians, Earth-Sci. Rev. 59 (2002) 77–100.
[20] S.M. McLennan, S. Hemming, Samarium/neodymium elemental and isotopic systematics in sedimentary rocks, Geochim. Cosmochim. Acta 56 (1992) 887–898.
[21] X. Liu, D.R. Fu, P.Y. Yao, G.F. Liu, N.W. Wang, Stratigraphy, Paleogeography, and Sedimentary-tectonic Development of Qinghai–Xizang Plateau, Geol. Publ. House, Beijing, 1992, 168 pp.
[22] J.Q. Huang, B.W. Chen, The Evolution of the Tethys in China and Adjacent Regions, Geol. Publ. House, Beijing, 1987, 109 pp.
[23] K.J. Zhang, Y.X. Zhang, B.D. Xia, Y.B. He, Temporal variations of the Mesozoic sandstone composition in the Qiangtang block, northern Tibet (China): implications for provenance and tectonic setting, J. Sediment. Res. 76 (2006), doi:10.2110/jsr.2006.089.
[24] K.J. Zhang, B.D. Xia, X.W. Liang, Mesozoic and Paleogene sedimentary facies and paleogeography of Tibet: tectonic implications, Geol. J. 37 (2002) 217–246.
[25] D.L. Sun, On the Permian biogeographic boundary between Gondwanan and Eurasia in Tibet, China as the eastern section of the Tethys, Palaeogeogr. Palaeoclimatol. Palaeoecol. 100 (1993) 59–77.
[26] J. Yin, J. Xu, C. Liu, H. Li, The Tibetan plateau: regional stratigraphic context and previous work, Philos. Trans. R. Soc. Lond. A 327 (1988) 5–52.
[27] K.J. Zhang, Blueschist-bearing metamorphic core complexes in the Qiangtang terrain reveal deep crustal structure of northern Tibet: comment, Geology 29 (2001) 90.
[28] K.J. Zhang, Cretaceous paleogeography of Tibet and adjacent areas (China): tectonic implication, Cretac. Res. 21 (2000) 23–33.
[29] T.Y. Guo, D.Y. Liang, Y.Z. Zhang, C.H. Zhao, Geology of Ngari, Tibet (Xizang), China, China Univ. Geosci. Press, Wuhan, 1991, 464 pp.
[30] J.W. Cowie, M.G. Bassett, Global Stratigraphic Chart, International Union of Geological Sciences, Bureau of International Commission on Stratigraphy, 1989.
[31] X.R. Liang, G.J. Wei, X.H. Li, Y. Liu, Precise measurement of $^{143}Nd/^{144}Nd$ and Sm/Nd ratios using multiple-collectors inductively coupled plasma-mass spectrometer (MS-ICPMS), Geochimica 32 (2003) 91–96.
[32] D.J. DePaolo, Neodymium isotopes in the Colorado Front Range and crust mantle evolution in the Proterozoic, Nature 291 (1981) 193–196.
[33] D.K. McDaniel, S.R. Hemming, S.M. McLennan, G.N. Hanson, Partial resetting of Nd isotopes and redistribution of REE during sedimentary processes: the Early Proterozoic Chelmsford Formation, Sudbury Basin, Ontario, Canada, Geochim. Cosmochim. Acta 58 (1994) 931–941.
[34] M. Ohr, A.N. Halliday, D.R. Peacor, Sr and Nd isotopic evidence for punctuated clay diagenesis. Texas Gulf Coast, Earth Planet. Sci. Lett. 105 (1991) 110–126.
[35] D.N. Awwiller, L.E. Mack, Diagenetic modification of Sm–Nd model ages in Tertiary sandstones and shales, Texas Gulf Coast, Geology 19 (1991) 311–314.
[36] S.L. Goldstein, R.K. O'Nions, P.J. Hamilton, A Sm–Nd isotopic study of atmospheric dusts and particulates from major river systems, Earth Planet. Sci. Lett. 70 (1984) 221–236.
[37] S.J. Goldstein, S.B. Jacobsen, Nd and Sr isotopic systematics of river water suspended material: implications for crustal evolution, Earth Planet. Sci. Lett. 87 (1988) 249–265.
[38] S.B. Jacobsen, Isotopic constraints on crustal growth and recycling, Earth Planet. Sci. Lett. 90 (1988) 315–329.
[39] C.J. Allègre, D. Rousseau, The growth of the continent through geological time studied by Nd isotope analysis of shales, Earth Planet. Sci. Lett. 67 (1984) 19–34.
[40] N.B.W. Harris, R.H. Xu, C.L. Lewis, C.J. Hawkesworth, Y.Q. Zhang, Isotope geochemistry of the 1985 Tibet Geotraverse, Lhasa to Golmud, Philos. Trans. R. Soc. Lond. A 327 (1988) 263–285.
[41] M.G. Zhang, C.Z. Hu, R.Z. Wu, C.S. Wang, Petrochemistry and tectonic setting of Xiangqiong–Chasan basic volcanic rocks in northern Xizang (Tibet), Contrib. Geol. Qinghai–Xizang (Tibet) Plateau, vol. 9, 1985, pp. 57–68.
[42] P.M. Myrow, N.C. Hughes, T.S. Paulsen, I.S. Williams, S.K. Parcha, K.R. Thompson, S.A. Bowring, S.C. Peng, A.D. Ahluwalia, Integrated tectonostratigraphic analysis of the Himalaya and implications for its tectonic reconstruction, Earth Planet. Sci. Lett. 212 (2003) 433–441.
[43] R.R. Parrish, K.V. Hodges, Isotopic constraints on the age and provenance of Lesser and Greater Himalayan sequences, Nepalese Himalaya, Geol. Soc. Amer. Bull. 108 (1996) 904–911.

[44] D.M. Robinson, P.G. DeCelles, P.J. Patchett, C.N. Garzione, The kinematic evolution of the Nepalese Himalaya interpreted from Nd isotopes, Earth Planet. Sci. Lett. 192 (2001) 507–521.
[45] P.G. DeCelles, G.E. Gehrels, J. Quade, B.N. Lareau, M.S. Spurlin, Tectonic implications of U–Pb zircon ages of the Himalayan orogenic belt in Nepal, Science 288 (2000) 497–499.
[46] R.H. Xu, U. Schärer, C.J. Allègre, Magmatism and metamorphism in the Lhasa block (Tibet): a geochronological study, J. Geol. 93 (1985) 41–57.
[47] C.S. Wang, C.Z. Hu, R.Z. Wu, Discovery and geologic significance of the Casang–Cabu rift in northern Xizang, Bull. Chengdu Coll. Geol. 14 (1987) 33–46.
[48] O. Bruguier, J.R. Lancelot, J. Malavieille, U–Pb dating on single detrital zircon grains from the Triassic Songpan–Ganze Flysch (central China): provenance and tectonic correlations, Earth Planet. Sci. Lett. 152 (1997) 217–231.
[49] Z.Q. Liu, et al., Tectonics, Geological Evolution and Genetic Mechanism of Qinghai–Xizang Plateau, Geol. Publ. House, Beijing, 1990, 174 pp.
[50] A. Dia, C.J. Allègre, A.J. Erlank, The development of continental crust through geological time: the South African case, Earth Planet. Sci. Lett. 98 (1990) 74–89.
[51] Y.X. Zhang, K.J. Zhang, B. Li, Y. Wang, Q.G. Wei, X.C. Tang, Zircon SHRIMP U–Pb geochronology and petrogenesis of the plagiogranites from the Laguoco ophiolite, Gaize, Tibet, Chinese, Sci. Bull. 52 (2007) 651–659.
[52] J.A. Pearce, H. Mei, Volcanic rocks of the 1985 Tibet geotraverse. Lhasa to Golmud, Philos. Trans. R. Soc. Lond., A 327 (1988) 169–201.
[53] N.B.W. Harris, S. Inger, R.H. Xu, Cretaceous plutonism in central Tibet: an example of post-collision magmatism? J. Volcanol. Geotherm. Res. 44 (1990) 21–32.
[54] C. Miller, R. Schuster, U. Klotzli, W. Frank, B. Grasemann, Late Cretaceous–Tertiary magmatic and tectonic events in the Transhimalaya batholith (Kailas area, SW Tibet), Schweiz. Mineral. Petrogr. Mitt. 80 (2000) 1–20.
[55] X.B. Wang, P.S. Bao, W.M. Deng, F.G. Wang, Xizang (Tibet) Ophiolites, Geol. Publ. House, Beijing, 1987, 336 pp.
[56] P. Stille, N. Clauer, J. Abrecht, Nd isotopic composition of Jurassic Tethys seawater and the genesis of Alpine Mn-deposits: evidence from Sr–Nd isotope data, Geochim. Cosmochim. Acta 53 (1989) 1095–1099.
[57] G. Davies, A. Gledhill, C. Hawkesworth, Upper crustal recycling in southern Britain: evidence from Nd and Sr isotopes, Earth Planet. Sci. Lett. 75 (1985) 1–12.
[58] C.J. Allègre, D. Rousseau, The growth of continent through geological time studied by Nd isotope analysis of shales, Earth Planet. Sci. Lett. 67 (1984) 19–34.